

# Spatio-Temporal Token Pruning for Efficient High-Resolution GUI Agents

Zhou Xu  
Tsinghua University  
Shenzhen, China  
xu-z25@mails.tsinghua.edu.cn

Bowen Zhou  
Tsinghua University  
Shenzhen, China  
zhoubw25@mails.tsinghua.edu.cn

Qi Wang  
Xidian University  
Xi'an, China  
qiwang0720@stu.xdu.edu.cn

Shuwen Feng  
Tsinghua University  
Shenzhen, China  
fsw25@mails.tsinghua.edu.cn

Jingyu Xiao\*  
The Chinese University of Hong Kong  
Hong Kong, China  
jyxiao@link.cuhk.edu.hk

## Abstract

Pure-vision GUI agents provide universal interaction capabilities but suffer from severe efficiency bottlenecks due to the massive spatiotemporal redundancy inherent in high-resolution screenshots and historical trajectories. We identify two critical misalignments in existing compression paradigms: the *temporal mismatch*, where uniform history encoding diverges from the agent’s “fading memory” attention pattern, and the *spatial topology conflict*, where unstructured pruning compromises the grid integrity required for precise coordinate grounding, inducing spatial hallucinations. To address these challenges, we introduce **GUIPruner**, a training-free framework tailored for high-resolution GUI navigation. It synergizes **Temporal-Adaptive Resolution (TAR)**, which eliminates historical redundancy via decay-based resizing, and **Stratified Structure-aware Pruning (SSP)**, which prioritizes interactive foregrounds and semantic anchors while safeguarding global layout. Extensive evaluations across diverse benchmarks demonstrate that GUIPruner consistently achieves state-of-the-art performance, effectively preventing the collapse observed in large-scale models under high compression. Notably, on Qwen2-VL-2B, our method delivers a 3.4× reduction in FLOPs and a 3.3× speedup in vision encoding latency while retaining over 94% of the original performance, enabling real-time, high-precision navigation with minimal resource consumption.

## CCS Concepts

• **Computing methodologies** → **Artificial intelligence**.

## Keywords

GUI Agents, Token Compression, MLLMs

\*Jingyu Xiao is the corresponding author.

Permission to make digital or hard copies of all or part of this work for personal or classroom use is granted without fee provided that copies are not made or distributed for profit or commercial advantage and that copies bear this notice and the full citation on the first page. Copyrights for components of this work owned by others than the author(s) must be honored. Abstracting with credit is permitted. To copy otherwise, or republish, to post on servers or to redistribute to lists, requires prior specific permission and/or a fee. Request permissions from [permissions@acm.org](mailto:permissions@acm.org).  
*Conference acronym 'XX, Woodstock, NY*

© 2018 Copyright held by the owner/author(s). Publication rights licensed to ACM.  
ACM ISBN 978-1-4503-XXXX-X/2018/06  
<https://doi.org/XXXXXXXX.XXXXXXX>

## ACM Reference Format:

Zhou Xu, Bowen Zhou, Qi Wang, Shuwen Feng, and Jingyu Xiao. 2018. Spatio-Temporal Token Pruning for Efficient High-Resolution GUI Agents. In *Proceedings of Make sure to enter the correct conference title from your rights confirmation email (Conference acronym 'XX)*. ACM, New York, NY, USA, 18 pages. <https://doi.org/XXXXXXXX.XXXXXXX>

## 1 Introduction

The evolution of Multimodal Large Language Models (MLLMs) has fundamentally reshaped the landscape of Graphical User Interface (GUI) agents. Traditional GUI agents [4, 5, 9, 31, 32] typically rely on textual representations such as HTML or accessibility trees, which are often plagued by noise, excessive sequence lengths, and the requirement for intrusive system-level permissions [8, 56]. In contrast, pure-vision-based GUI agents [8, 15, 40, 41, 50, 55] act by directly analyzing screenshots, effectively mimicking human interaction. This paradigm shift empowers agents with robust universality across diverse applications and platforms.

Despite the promising universality of vision-based GUI agents, their efficiency is severely constrained by the spatiotemporal redundancy inherent in contextual modeling. We analyze element and history contexts to uncover two critical challenges that existing methods fail to address. 1) **The mismatch between high historical resolution and low attention**. As illustrated in Figure 1 (Top), conventional methods typically enforce uniform high-resolution encoding across the entire history, disregarding the temporal dynamics of agent perception. Our analysis, however, reveals a distinct “**Temporal Decay**” pattern: attention is heavily concentrated on recent frames (the “Recency Effect”) while distant history receives negligible weight. Consequently, the prevailing “high resolution, low attention” configuration incurs massive computational waste, as distant frames necessitate only semantic outlines rather than pixel-level fidelity. 2) **The conflict between token sparsity and spatial topology**. GUI screenshots are highly sparse, with background tokens often dominating the visual context, accounting for over 60%. While theoretically compressible, specific background regions (e.g., layout boundaries) serve as essential semantic anchors. Existing general-purpose compression methods [1, 7, 24, 53] often employ unstructured pruning strategies (Figure 1, Top Right). Such destructive operations cause two major issues: they disrupt the inherent 2D grid structure required for accurate coordinates grounding, inducing severe “**spatial hallucinations**”, and they

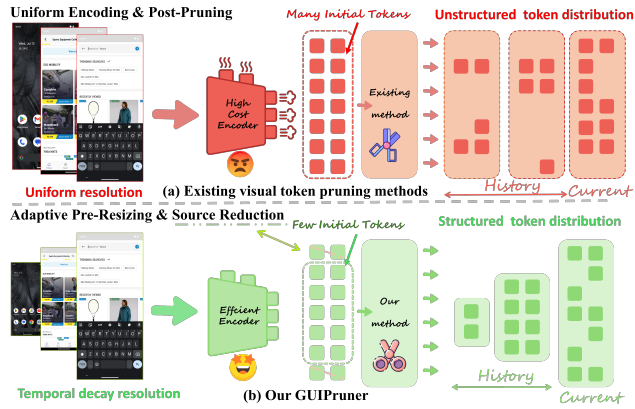


**Figure 1: Paradigm comparison of visual encoding and pruning.** In contrast to conventional pipelines (Top) that incur high redundancy via uniform encoding and disrupt topology via unstructured pruning, GUIPruner (Bottom) implements efficient source-level reduction and structured, topology-preserving compression, ensuring high-precision grounding with minimal token consumption.

indiscriminately discard structurally meaningful regions, leading to degraded reasoning and potential task failures.

To address these challenges, we propose **GUIPruner**, a framework tailored for high-resolution GUI navigation. The framework synergizes two modules **Temporal-Adaptive Resolution (TAR)** and **Stratified Structure-aware Pruning (SSP)** to efficiently compress historical and element contexts, respectively. First, to mitigate historical redundancy, we propose **TAR**, a global-to-local resource scheduling mechanism. Departing from prior works that treat historical frames independently [6, 29], TAR mimics the biological “fading memory” by imposing a holistic token budget distributed across the temporal dimension. As depicted in Figure 1 (Bottom Left), we employ a linear decay scheme to allocate token quotas, ensuring resolution monotonically attenuates with temporal distance. Crucially, this pre-computation resizing suppresses token generation at the source, directly curtailing the vision encoder’s computational overhead. This mechanism effectively eliminates pixel-level redundancy in distant history while preserving high-fidelity details for the immediate context. Second, to reconcile the trade-off between token sparsity and spatial topology, we propose **SSP**, which operates within the shallow layers of the MLLM. Instead of unstructured pruning that disrupts spatial grids (Figure 1, Top Right), SSP employs a Stratified Budget Allocation Strategy to hierarchically partition the visual context. It prioritizes: (1) preserving high-resolution features of interactive foreground targets (e.g., buttons, input box); (2) retaining semantically salient background regions via attention ranking; and (3) dedicating the residual budget to Uniform Grid Sampling (UGS) (Figure 1, Bottom Right). UGS acts as a structural safeguard, maintaining a coarse-grained perception of the global layout to prevent “spatial hallucinations”.

We validate the effectiveness of GUIPruner through rigorous benchmarking against state-of-the-art training-free methods. Evaluated across four diverse datasets (AITW [34], Mind2Web [13], GUI-Odyssey [29], AndroidControl [22]) and varying model scales

(Qwen2-VL-2B [42] and Qwen2.5-VL-7B [2]), our results confirm its superior robustness. Notably, on the challenging Mind2Web, GUIPruner consistently maintains SOTA performance across varying compression ratios and effectively mitigates the catastrophic collapse observed in Qwen2.5-VL-7B. In terms of efficiency, it achieves a  $3.4\times$  FLOPs reduction and  $3.3\times$  encoder speedup on Qwen2-VL-2B, enabling real-time, high-resolution navigation with minimal resource consumption.

The main contributions are summarized as follows:

- We dissect the spatiotemporal redundancy in GUI agents, identifying “Temporal Decay” in history and the “Sparsity-Topology Conflict” in the current frame as critical bottlenecks. This analysis uncovers the fundamental limitations of uniform compression paradigms in coordinate-sensitive grounding tasks.
- We propose **GUIPruner**, a plug-and-play visual compression framework. By synergizing **Temporal-Adaptive Resolution (TAR)** and **Stratified Structure-aware Pruning (SSP)**, our approach dynamically aligns visual encoding with the agent’s spatiotemporal cognitive patterns, eliminating redundancy without requiring parameter updates.
- GUIPruner consistently achieves state-of-the-art performance across diverse benchmarks, effectively mitigating the performance collapse observed in large-scale (7B) models. Empirically, it delivers a  $3.4\times$  **FLOPs reduction** and a  $3.3\times$  **speedup** on Qwen2-VL-2B, enabling efficient real-time deployment.

## 2 Related Work

**GUI Agents.** The development of GUI agents [30, 43] has transitioned from pipeline-based systems relying on auxiliary tools (e.g., Accessibility Trees, OCR) [20, 25, 44, 45, 51, 52] to end-to-end multimodal models trained on visual corpora. While removing dependencies on inaccessible metadata [40, 50], these models incur high computational costs due to the necessity of processing high-resolution inputs and long interaction histories. To mitigate this burden, recent studies have explored various efficiency mechanisms. OdysseyAgent [29] proposes a history resampling module to compress past screenshots, though this introduces additional learnable parameters. Iris [14] and ShowUI [26] attempt to filter redundant backgrounds using low-level visual cues; however, Iris is restricted to current-frame inputs, while ShowUI suffers from notable performance degradation during inference. Similarly, SimpAgent [6] and GUI-Rise [28] employ consistency-guided training or reinforcement learning to summarize historical interactions. In contrast, we propose a training-free visual compression framework explicitly designed to preserve GUI structural integrity, achieving high efficiency without parameter updates.

**Visual Token Pruning.** Multimodal Large Language Models (MLLMs) are crucial for handling complex real-world tasks (e.g., image understanding [27], code generation [11, 38, 47?–49], structural visual design [37], testing agents [39]), yet processing high-resolution images imposes a heavy computational burden. While some approaches [10, 18, 21, 23, 54] compress tokens using learnable queries (which require extra training), the research focus has shifted toward training-free pruning methods that work directly during inference. State-of-the-art methods generally optimize token selection through different strategies: *FastV* [7] filters out tokens

with low attention scores in shallow layers. In contrast, *DivPrune* [1] formulates pruning as a Max-Min Diversity Problem (MMDP) [35] to select the most diverse subset of tokens. Similarly, methods like *MoB* [24] and *CDPruner* [53] further refine this by aligning tokens with text prompts or using Determinantal Point Processes (DPP) [19]. However, these general methods are primarily designed for natural images. They often fail to preserve the dense and structured layouts typical of Graphical User Interfaces (GUIs). To address this, we propose a specialized compression method that effectively captures the unique structural characteristics of GUIs, resolving the limitations of existing approaches.

### 3 Preliminary

#### 3.1 Problem Formulation

We formalize the interaction between the GUI agent and the digital environment as an autoregressive trajectory generation process. Given a global user instruction  $\mathcal{I}$ , the agent operates within a discrete time horizon to autonomously accomplish the task. At each time step  $t$ , the agent’s policy  $\pi$  integrates a multimodal input stream consisting of the static instruction  $\mathcal{I}$ , the current visual state  $X_t$ , and a retrospective context  $\mathcal{H}_t$  to predict the subsequent action  $a_t$  (e.g., precise click coordinates). Formally, the history  $\mathcal{H}_t$  comprises a sequence of interleaved past observations and actions, denoted as  $\mathcal{H}_t = \{(X_{t-k}, a_{t-k})\}_{k=1}^T$ , where  $T$  represents the maximum temporal window size. While this historical trajectory provides essential contextual cues for tracking execution progress, it simultaneously induces a massive accumulation of visual tokens, which significantly impedes efficient real-time inference.

#### 3.2 Redundancy of Historical Visual Tokens

During GUI action prediction, incorporating historical information is crucial for the agent to comprehend the current task, particularly within complex graphical interfaces where historical context aids in making robust decisions. Prior research, such as *SimpAgent* [6], indicates that while the current observation is the dominant factor for action prediction, the inclusion of historical observations further improves models’ performance. However, this improvement comes at a significant computational cost, as historical context introduces a large number of additional visual tokens, thereby substantially increasing inference overhead.

Historical information functions analogously to task working memory. Human Visual Working Memory (VWM) exhibits a significant “**Recency Effect**” [57], where clear details are retained for recent scenes, while only fuzzy semantic outlines are preserved for distant memories. To investigate whether Multimodal Large Language Models (MLLMs) possess similar characteristics, we visualize the Cross-Attention weights distribution of the agent regarding historical frames during multi-step decision-making processes (as shown in Figure 2(a)).

We observe a pronounced **Temporal Decay** phenomenon: the agent’s attention is heavily concentrated on the most recent 1 ~ 2 frames to capture the immediate interaction state. Conversely, as the time lag increases, the attention weights assigned to historical frames gradually diminish. However, existing GUI agents overlook this pattern, enforcing a uniform high-resolution encoding for all historical frames regardless of their temporal distance. The “high

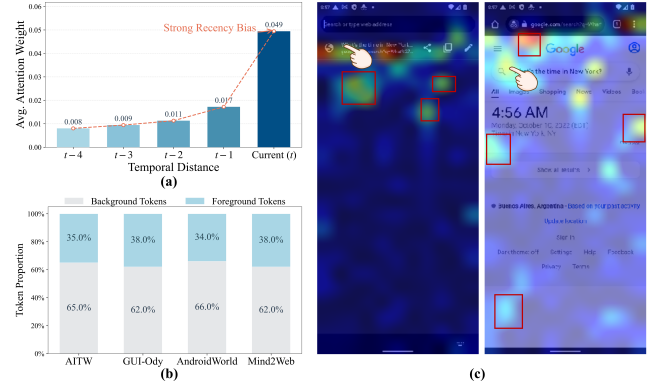


**Figure 2: (a) Cross-attention weights exhibit a pronounced *Temporal Decay*, consistent with the “Recency Effect” in working memory. (b) Background tokens dominate the visual context across four datasets, indicating significant spatial redundancy. (c) Heatmaps reveal that specific background regions (red boxes) retain high attention as essential semantic anchors, cautioning against indiscriminate pruning.**

resolution, low attention” configuration results in severe computational waste. This observation inspires our **Dynamic Resolution Strategy**, which adaptively decays the input resolution as the time lag increases, eliminating pixel-level redundancy while mimicking biological memory mechanisms.

**Observation 1:** MLLMs’ attention over GUI histories decays sharply over time, making uniform high-resolution encoding of distant frames inefficient.

#### 3.3 Redundancy of Current Frame

To investigate the potential for compressing the current frame, we first conduct a quantitative analysis of visual token composition in high-resolution GUI screenshots. As illustrated in Figure 2(b), due to the inherent sparsity of GUI layouts, background tokens predominantly occupy the visual context (often exceeding 60%), while foreground tokens representing interactive elements constitute only a minor fraction. This extreme imbalance reveals substantial computational redundancy. However, this does not imply that background tokens can be indiscriminately discarded. By visualizing the attention distribution (as shown in Figure 2(c)), we observe that specific background regions, particularly those layout references, retain high attention scores, suggesting that naive background removal risks stripping away essential semantic context.

Crucially, we must address the stringent spatial requirements of GUI tasks. Unlike general visual question answering, GUI agents typically need to output precise pixel coordinates  $(x, y)$ , which heavily depends on the integrity of 2D spatial positional encodings. Existing research [26] indicates that unstructured token pruning disrupts the original grid integrity of the image. This topological degradation impairs the agent’s perception of relative element positions, thereby inducing “spatial hallucinations” in coordinate prediction. Consequently, an effective compression strategy must

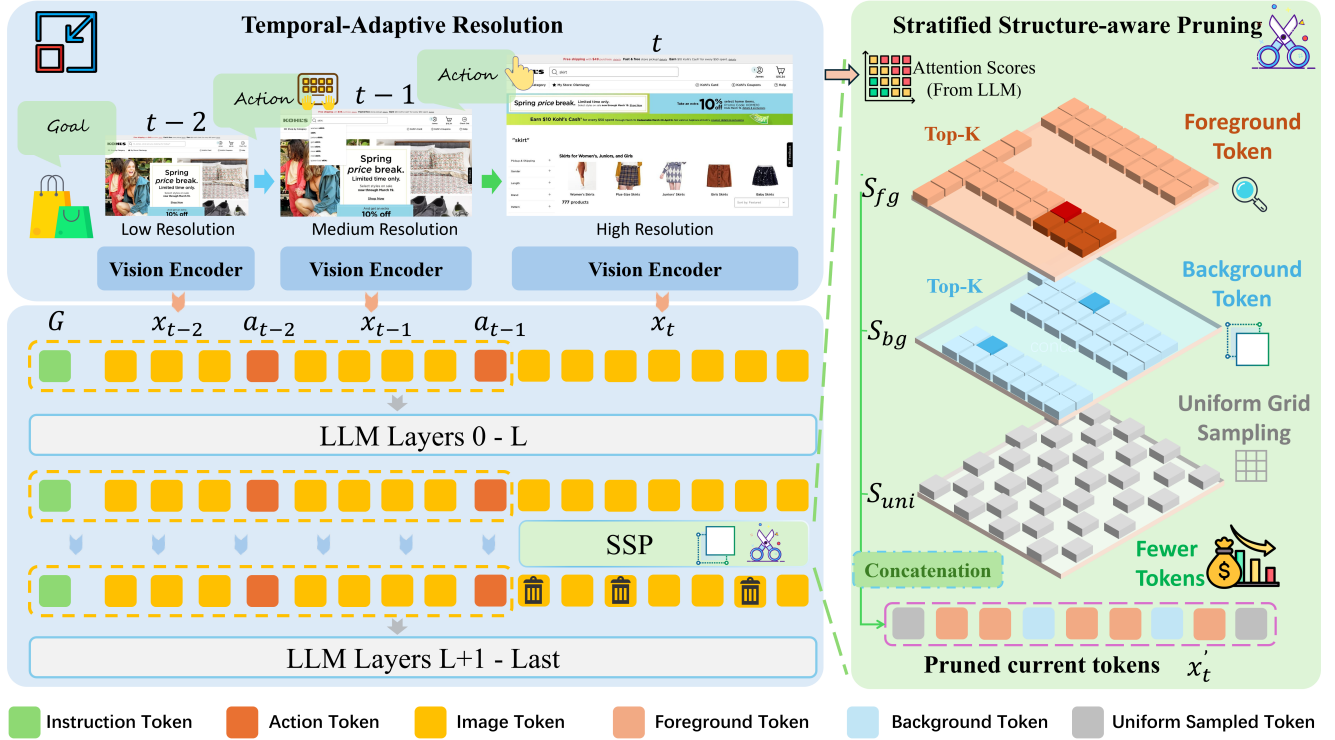


**Figure 3: Overview of the GUIPruner framework.** The framework addresses spatiotemporal redundancy through two synergistic modules: (Left) **Temporal-Adaptive Resolution (TAR)** mimics biological fading memory by assigning decaying resolution budgets to historical frames based on temporal distance, eliminating redundancy in distant context. (Right) **Stratified Structure-aware Pruning (SSP)** operates on the current frame within shallow LLM layers. It preserves topological integrity by hierarchically retaining interactive foreground tokens ( $S_{fg}$ ), semantic background anchors ( $S_{bg}$ ), and a uniform structural grid ( $S_{uni}$ ), effectively compressing visual tokens without inducing spatial hallucinations.

satisfy two requirements: it should drastically reduce background redundancy while strictly preserving the topological structure of the spatial grid to ensure accurate grounding.

**Observation 2:** Current GUI frames exhibit extreme background redundancy, yet naive token pruning risks disrupting spatial structure and inducing “spatial hallucinations,” highlighting the need for topology-preserving compression.

## 4 Methodology

### 4.1 Overview

In this section, we detail our proposed framework, GUIPruner, as shown in Figure 3. We introduce two novel mechanisms: **Temporal-Adaptive Resolution (TAR, §4.2)** for eliminating pixel-level redundancy in historical contexts, and **Stratified Structure-aware Pruning (SSP, §4.3)** for efficient, topology-preserving encoding of the current interactive state.

### 4.2 Temporal-Adaptive Resolution

To address the temporal redundancy identified in Section 3.2, we propose the **Temporal-Adaptive Resolution (TAR)** mechanism

to dynamically allocate resolution for historical frames. Unlike prior works that treat history frames independently, our method adopts a global-to-local resource scheduling mechanism. It first imposes a holistic constraint on the total computational budget and then distributes this budget across the temporal dimension, mimicking the biological “fading memory” where information density decays as time goes by.

**Global Budget Formulation.** Formally, let the history context at time step  $t$  be denoted as  $\mathcal{H}_t = \{X_{t-1}, X_{t-2}, \dots, X_{t-T}\}$ , where  $X_{t-k}$  represents the frame with a temporal lag  $k$ . To strictly control the computational overhead, we introduce a global hyperparameter  $\lambda \in (0, 1]$ , termed the History Token Retention Ratio. Given the standard token count per frame  $N_{orig} = \frac{HW}{p^2}$  (where  $P$  is the patch size, assuming uniform resolution  $H \times W$ ), the total allowable token budget  $N_{budget}$  for the entire history sequence is constrained by:

$$N_{budget} = \lfloor T \times N_{orig} \times \lambda \rfloor, \quad (1)$$

which ensures that the agent’s memory footprint is bounded by a user-defined ratio  $\lambda$ , regardless of the history length  $T$ .

**Temporal-decay Token Allocation.** We distribute the global budget  $N_{budget}$  via a Linear Decay Schedule governed by a retention factor  $\gamma \in (0, 1]$ . Formally, we define the unnormalized importance weight  $w_k$  (interpolating from 1 down to  $\gamma$ ) and the final allocated

token quota  $n_k$  as:

$$w_k = \gamma + (1 - \gamma) \frac{T - k}{T - 1}, \quad n_k = N_{budget} \cdot \frac{w_k}{\sum_{j=1}^T w_j}. \quad (2)$$

This strategy smoothly attenuates resolution for distant frames, allocating higher fidelity to recent observations while preserving minimal context via  $\gamma$ .

**Resolution Mapping.** To strictly enforce the allocated token budget  $n_k$ , we map the discrete quota back to the continuous spatial domain. Given that the token count in ViTs [16] scales quadratically with image resolution, we derive the scaling factor  $s_k$  for frame  $X_{t-k}$  as:

$$s_k = \sqrt{\frac{n_k}{N_{orig}}}. \quad (3)$$

Accordingly, the frame  $X_{t-k}$  is resized to  $(s_k H, s_k W)$  via bilinear interpolation. This simple projection ensures the actual computational cost aligns with our schedule without introducing any learnable parameters.

### 4.3 Stratified Structure-aware Pruning

To reconcile the efficiency bottleneck of high-resolution inputs with the strict topological requirements of GUI grounding, we propose **Stratified Structure-aware Pruning (SSP)**. Implemented within the shallow layers of the MLLM, SSP serves as an early-stage structural sieve that refines visual representations before they propagate to deeper reasoning blocks. Unlike prior methods [1, 7, 24, 53] relying solely on attention scores (which degrade spatial grids) or static priors (which neglect semantic context), SSP dynamically balances foreground regions containing interactive elements, background regions with semantic salience, and global topology under a strict token budget.

**Importance Estimation and Partitioning.** Given the visual token sequence  $\mathcal{T}$  derived from the current frame, we first partition it into a foreground set  $\mathcal{T}_{fg}$  and a background set  $\mathcal{T}_{bg}$  via edge detection. We then derive an importance score  $s_i$  for each token  $t_i$  using aggregated attention weights from the shallow transformer layers. By coupling explicit structural priors with implicit attention-based saliency, this step ensures that the pruning policy is conditioned on both the precise geometric boundaries of interactive elements and their semantic relevance.

**Stratified Retention Policy.** We introduce the Current Token Retention Ratio  $\mu \in (0, 1]$  to impose a global constraint on token usage. The total token budget is defined as  $K_{total} = \lfloor |\mathcal{T}| \times \mu \rfloor$ . To optimize the trade-off between compression and structural integrity, we allocate this budget across three hierarchical levels:

**(1) Foreground Saliency Preservation.** Since foreground regions typically encapsulate direct interaction targets, we prioritize the highest-attention tokens within  $\mathcal{T}_{fg}$ . We rank tokens by their score  $s_i$  and retain the top  $\mu$  fraction:

$$\mathcal{S}_{fg} = \text{TopK}(\mathcal{T}_{fg}, \lfloor |\mathcal{T}_{fg}| \times \mu \rfloor). \quad (4)$$

This ensures that high-resolution features of critical interactive components are fully preserved.

**(2) Background Semantic Retention.** To retain essential contextual cues, we introduce a background saliency factor  $\rho \in (0, 1]$ . We select the top  $\mu \cdot \rho$  fraction of background tokens  $\mathcal{T}_{bg}$  based on

attention ranking:

$$\mathcal{S}_{bg} = \text{TopK}(\mathcal{T}_{bg}, \lfloor |\mathcal{T}_{bg}| \times (\mu \cdot \rho) \rfloor). \quad (5)$$

This preserves semantic contexts vital for reasoning, even if they are not direct interaction targets.

**(3) Topological Structure Completion.** To avert the ‘‘spatial collapse’’ caused by unstructured pruning, we allocate the residual budget  $K_{res} = K_{total} - (|\mathcal{S}_{fg}| + |\mathcal{S}_{bg}|)$  to safeguard global structure. We apply Uniform Grid Sampling (UGS) on the remaining tokens  $\mathcal{T}_{remain} = \mathcal{T} \setminus (\mathcal{S}_{fg} \cup \mathcal{S}_{bg})$ :

$$\mathcal{S}_{uni} = \text{UGS}(\mathcal{T}_{remain}, K_{res}). \quad (6)$$

This mechanism maintains a coarse-grained representation of the global layout and relative positioning, effectively preventing spatial hallucinations during coordinate grounding.

**Outcome.** The final compressed sequence  $\mathcal{T}_{final} = \mathcal{S}_{fg} \cup \mathcal{S}_{bg} \cup \mathcal{S}_{uni}$  reduces computational overhead in deep layers while rigorously preserving the 2D spatial integrity required for precise navigation. To intuitively illustrate this mechanism, we provide a detailed visualization of the SSP process in Appendix C.

## 5 Experiments

### 5.1 Experimental Setup

**Base Models.** To evaluate the scalability and effectiveness of our proposed framework, we employ Qwen2-VL-2B [42] and Qwen2.5-VL-7B [2] as our foundational Multimodal Large Language Models (MLLMs). To align these general-purpose models with the specific input-output modalities of GUI navigation tasks, we perform supervised fine-tuning on the target datasets. During inference, we configure the sampling temperature to 0.01 for Qwen2-VL-2B and  $10^{-6}$  for Qwen2.5-VL-7B. Regarding the specific hyperparameters of our method, we set  $\gamma = 0.2$  and  $\rho = 0.3$ . Comprehensive implementation details regarding the fine-tuning process and additional experimental settings are provided in Appendix A.4.

**Datasets.** We validate the robustness of our method across four diverse benchmarks, all characterized by long-horizon interactions and sequential visual history. These datasets span distinct GUI ecosystems: GUI-Odyssey, AndroidControl, and AITW represent the extensive Mobile domain, while Mind2Web serves as a rigorous benchmark for the Web domain.

**Comparative Methods.** We benchmark against state-of-the-art training-free baselines spanning diverse pruning criteria and execution stages. We evaluate Pre-LLM methods, specifically DivPrune [1] and CDPruner [53], which reduce tokens prior to model input. For In-LLM methods, we include FastV [7] and MoB [24], which perform pruning during the inference process.

### 5.2 Research Questions

- **RQ1 (Performance & Scalability):** Can GUIPruner effectively compress visual tokens while preserving or even enhancing navigation performance across diverse GUI domains (Mobile, Web) and varying model scales?
- **RQ2 (Efficiency):** What are the tangible computational benefits of GUIPruner about FLOPs reduction, inference acceleration, and GPU memory overhead compared to SOTA pruning baselines?

**Table 1: Performance benchmarking on GUI navigation tasks. We evaluate Qwen2-VL-2B and Qwen2.5-VL-7B across three pruning settings. Abbreviations: “GUI-Ody” (GUI-Odyssey), “M2Web” (Mind2Web), and “AndCtrl” (AndroidControl).**

Method	Qwen2-VL-2B				Qwen2.5-VL-7B			
	AITW	M2Web	GUI-Ody	AndCtrl	AITW	M2Web	GUI-Ody	AndCtrl
<i>Upper Bound (Full Tokens)</i>								
Original Model	69.5	34.5	71.8	66.9	71.2	35.2	78.4	71.6
<i>Setting I: Retain History 40% / Current 75%</i>								
FastV (ECCV'24)	66.2	33.4	67.3	66.3	67.9	34.3	73.5	70.8
DivPrune (CVPR'25)	65.3	22.8	67.1	65.6	23.2	7.7	13.6	29.4
CDPruner (NeurIPS'25)	64.3	18.3	65.1	61.8	23.0	6.8	13.8	29.2
MoB (NeurIPS'25)	66.5	21.0	66.8	65.0	68.8	32.7	74.0	71.1
<b>GUIPruner</b>	<b>67.5</b>	<b>33.6</b>	<b>68.1</b>	<b>66.4</b>	<b>69.4</b>	<b>34.7</b>	<b>74.4</b>	<b>71.3</b>
<i>Setting II: Retain History 20% / Current 75%</i>								
FastV (ECCV'24)	64.2	32.4	64.9	65.4	66.6	33.6	70.3	70.0
DivPrune (CVPR'25)	63.7	21.8	64.0	64.4	20.3	6.3	11.6	24.4
CDPruner (NeurIPS'25)	63.2	18.0	63.1	60.6	20.7	6.7	11.3	24.5
MoB (NeurIPS'25)	64.9	20.3	64.2	64.0	66.7	31.9	70.4	70.4
<b>GUIPruner</b>	<b>66.3</b>	<b>32.9</b>	<b>66.3</b>	<b>65.9</b>	<b>67.9</b>	<b>34.1</b>	<b>73.0</b>	<b>70.9</b>
<i>Setting III: Retain History 10% / Current 75%</i>								
FastV (ECCV'24)	62.7	31.6	62.4	64.4	65.7	<b>33.1</b>	67.7	69.2
DivPrune (CVPR'25)	63.0	21.0	61.2	63.6	19.7	6.6	11.5	24.2
CDPruner (NeurIPS'25)	61.7	17.1	60.2	59.7	19.6	6.2	11.4	24.1
MoB (NeurIPS'25)	63.8	19.0	60.8	62.8	65.1	30.6	68.1	69.6
<b>GUIPruner</b>	<b>65.3</b>	<b>31.8</b>	<b>63.8</b>	<b>65.6</b>	<b>66.8</b>	32.8	<b>70.1</b>	<b>70.0</b>

- **RQ3 (Component Attribution):** How do the individual components: specifically Temporal-Adaptive Resolution (TAR) for history and Stratified Structure-aware Pruning (SSP) for the current frame—contribute to the overall robustness of the system?
- **RQ4 (Hyperparameter Sensitivity):** How do critical hyperparameters (e.g., temporal decay factor  $\gamma$ , background saliency factor  $\rho$ , and pruning layer depth  $L$ ) influence the trade-off between compression rate and grounding accuracy?

### 5.3 Overall Performance and Scalability (RQ1)

We evaluate our framework on Qwen2-VL-2B and Qwen2.5-VL-7B across four benchmarks under three history retention settings (10%, 20%, 40%, see Table 1). Recognizing the critical role of the current observation, we fix its token retention ratio at 75%. Our results demonstrate consistent superiority over state-of-the-art baselines, exhibiting robust scalability and adaptability.

**Universal Effectiveness on Lightweight Models.** On Qwen2-VL-2B, GUIPruner achieves comprehensive dominance across all datasets. Notably, on the challenging Mind2Web benchmark (Setting I), our method attains 33.6% accuracy, significantly outperforming diversity-based baselines like DivPrune (22.8%) and effectively matching the uncompressed upper bound (34.5%). This confirms

that combining pixel-level history downsampling with structure-aware pruning offers the most robust information retention for MLLMs with limited capacity.

**Mitigating Distribution Shift on Large-Scale Models.** On Qwen2.5-VL-7B, baselines like DivPrune and CDPruner suffer from catastrophic performance collapse, notably on Mind2Web (plummeting to 7.7% and 6.8%). We attribute this failure to their aggressive pre-LLM pruning, which discards tokens prior to input, severing spatiotemporal dependencies established during fine-tuning. In contrast, our approach circumvents this collapse (recovering 34.7% on Mind2Web) via a decoupled design: history is spatially downsampled to preserve global layout, while the current frame is pruned within shallow layers. This ensures the model initially perceives the complete visual context, maintaining alignment with the fine-tuned distribution before reducing redundancy, thereby safeguarding early-stage feature extraction.

**Resilience to High-Resolution Sparsity.** Mind2Web, distinguished by high-resolution viewports and sparse interactive elements, exposes the inherent limitations of metric-based pruning. As evidenced in Table 1, diversity or coverage-based methods (e.g., CDPruner, MoB) fail to identify effective tokens in sparse grids, yielding performance inferior to attention-based approaches. We incorporate attention priors to capture semantic relevance, yet unlike FastV’s unstructured filtering, we rigorously enforce topological

grid integrity. This strict constraint proves essential for preventing spatial misalignment during precise coordinate grounding in high-resolution GUIs, where unstructured selection typically fails.

## 5.4 Efficiency Analysis (RQ2)

We benchmark computational overhead against state-of-the-art pruning methods using Qwen2-VL-2B on a single NVIDIA RTX 4090, configured with  $N = 4$  history frames on AITW. As detailed in Table 2, with retention rates  $\lambda = 0.1$  and  $\mu = 0.75$ , our method achieves a **3.4× reduction in total FLOPs** (aggregated across vision encoding, prefill, and decoding phases). This theoretical reduction translates into tangible acceleration: we speed up the Vision Encoder and Prefill stages by **3.3×** and **1.9×**, respectively, effectively dismantling the visual encoding bottleneck. Additionally, our approach demonstrates exceptional resource efficiency, capping peak GPU memory at just 5.9 GB, thereby establishing a superior efficiency-performance trade-off. The efficiency analysis for Qwen2.5-VL-7B is provided in the Appendix E.

**Table 2: Efficiency comparison on Qwen2-VL-2B (AITW dataset, 4 history frames, RTX 4090). We report the number of tokens, FLOPs, Encoder latency, Prefill latency, and GPU memory usage. Bold indicates the best performance.**

Method	# Token	FLOPs (T)	Encoder Time (ms)	Prefill Time (ms)	GPU Memory (MB)
Qwen2-VL-2B	1320	11.5	87.9	47.5	8956
FastV	310	8.7 (×1.3)	87.9 (×1.0)	28.6 (×1.6)	6798
DivPrune	310	8.5 (×1.4)	87.9 (×1.0)	27.5 (×1.7)	6180
CDPruner	310	8.5 (×1.4)	87.9 (×1.0)	27.4 (×1.7)	6180
MoB	310	8.7 (×1.3)	87.9 (×1.0)	28.1 (×1.6)	6734
<b>GUIPruner</b>	310	<b>3.4 (×3.4)</b>	<b>26.6 (×3.3)</b>	<b>24.1 (×1.9)</b>	<b>5902</b>

## 5.5 Ablation Study (RQ3)

**5.5.1 Decoupled Analysis of TAR and SSP.** To meticulously dissect the individual contributions of our Temporal-Adaptive Resolution (TAR) and Stratified Structure-aware Pruning (SSP) modules, we conduct decoupled experiments using the Qwen2-VL-2B model. The 2B model was selected to isolate the efficacy of our compression strategies from the pre-training distribution shifts observed in larger 7B models. We evaluate our approach on two representative benchmarks: AITW (mobile) and Mind2Web (web). The four line charts in Figure 4 visualize the performance trajectories under varying compression intensities.

**Robustness of TAR.** We evaluated the efficacy of history compression by fixing the current frame retention at 100% and varying the history retention ratio  $\lambda$  across {10%, 20%, 40%} (Figure 4, left). Empirical results demonstrate that TAR consistently delivers superior performance across the entire compression spectrum. Notably, at a moderate retention ratio of 40%, our method achieves near-lossless performance on the AITW benchmark, closely approximating the uncompressed upper bound. More intriguingly, on Mind2Web, TAR even surpasses the original performance of the uncompressed model. This suggests that our “fading memory” mechanism not only preserves essential temporal dependencies but also effectively filters out irrelevant historical noise that may otherwise distract the agent.

**Resilience of SSP.** We assessed current frame compression by retaining the full history context and varying the current frame retention ratio  $\mu$  across {45%, 60%, 75%} (Figure 4, right). Results demonstrate that SSP consistently outperforms all baselines across compression levels. On the challenging Mind2Web benchmark, we observe two distinct failure modes in baselines. Metric-based pruners (e.g., MoB, CDPruner, DivPrune) suffer from catastrophic performance collapse, with accuracy languishing below 25%. While FastV maintains a relatively stable performance curve similar to ours, it consistently lags behind SSP, particularly in the low-retention regime (45%) where the gap widens. In contrast, SSP achieves the best trade-off, maintaining high accuracy even under aggressive compression. This confirms that explicitly preserving both foreground salience and the global topological grid is essential for precise coordinate grounding in high-resolution GUIs.

**5.5.2 TAR and SSP Deep Dive.** Using Qwen2-VL-2B on AITW and GUI-Odyssey, we validate TAR’s adaptive decay against uniform scaling and establish the necessity of SSP’s topological grid over random sampling.

**Effectiveness of Structural Components.** We isolate the contributions of the “fading memory” mechanism in TAR and the topological completion in SSP. (1) *Adaptive vs. Uniform History Resolution.* To validate the efficacy of our temporal decay strategy, we benchmark TAR against a Uniform Scaling baseline, which distributes the history budget equidistantly across all past frames. As detailed in Table 3, our adaptive strategy consistently outperforms the uniform baseline across varying retention ratios ( $\lambda \in \{10\%, 20\%, 40\%\}$ ). This confirms that allocating higher resolution to recent frames effectively aligns with the “recency bias” inherent in GUI interactions, whereas uniform allocation inefficiently expends computational resources on distant, stale contexts. (2) *Uniform Grid vs. Random Sampling.* To assess the necessity of topological completion in SSP, we replace the residual Uniform Grid Sampling (UGS) with random sampling while maintaining identical foreground and background retention. Results across current frame retention ratios ( $\mu \in \{45\%, 60\%, 75\%\}$ ) in Table 4 demonstrate the clear superiority of UGS. This verifies that preserving a deterministic, coarse-grained spatial skeleton is indispensable for preventing grounding hallucinations, whereas unstructured random sampling fails to uphold global layout integrity.

## 5.6 Parameter Study (RQ4)

Using Qwen2-VL-2B on AITW, we analyze the sensitivity of the temporal decay factor  $\gamma$ , the background saliency factor  $\rho$ , and the pruning layer depth  $L$ .

**Hyperparameter Sensitivity ( $\gamma, \rho$ ).** The results are visualized in Figure 5, which presents performance curves across three distinct compression rates.

(1) *Temporal Decay Factor  $\gamma$ .* With current frame retention fixed at 100%, we vary  $\gamma$ , the coefficient governing decay steepness ( $\gamma = 1.0$  signifies uniformity). As shown in Figure 5 (Left), performance peaks at  $\gamma = 0.2$  and monotonically degrades as  $\gamma \rightarrow 1.0$ . This confirms that prioritizing immediate history is superior to a uniform distribution, aligning with the agent’s reliance on high-fidelity recent context. (2) *Background Saliency Factor  $\rho$ .* Conversely, with history frames fully retained to isolate spatial effects, we analyze  $\rho$ ,

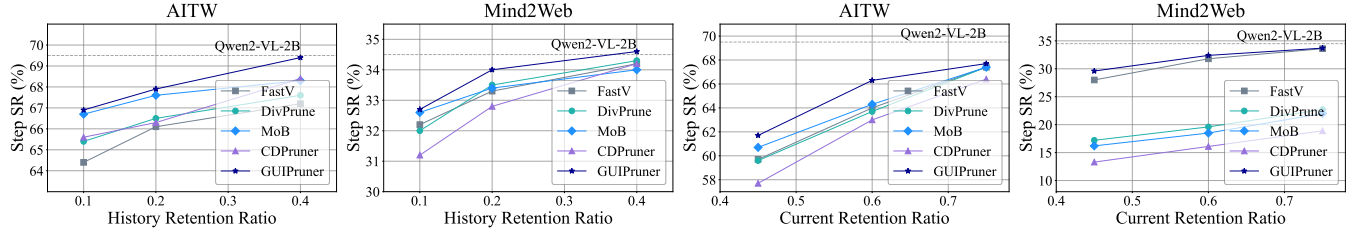


**Figure 4: Decoupled sensitivity analysis of TAR and SSP on Qwen2-VL-2B. Left: Evaluation of TAR under varying history retention ratios ( $\tau$ ) on AITW and Mind2Web. Right: Evaluation of SSP under varying current frame retention ratios ( $\kappa$ ). GUIPruner consistently demonstrates superior robustness over baselines, particularly in high-compression regimes.**

**Table 3: History token allocation ablation. We compare our proposed decay-based strategy (TAR) against a uniform allocation baseline across varying history budgets. "Rel." denotes performance relative to the full-context upper bound.**

Method	AITW	GUI-Ody	Avg.	Rel.
Qwen2-VL-2B	<i>Upper Bound (Full Tokens)</i>			
Vanilla	69.5	71.8	70.6	100%
Qwen2-VL-2B	<i>Retain History 40% / Current 100%</i>			
TAR w/ Uniform	68.4	70.2	69.3	98.2%
<b>TAR (Ours)</b>	<b>69.4</b>	<b>70.6</b>	<b>70.0</b>	<b>99.2%</b>
Qwen2-VL-2B	<i>Retain History 20% / Current 100%</i>			
TAR w/ Uniform	67.0	67.4	67.2	95.2%
<b>TAR (Ours)</b>	<b>67.9</b>	<b>68.7</b>	<b>68.3</b>	<b>96.7%</b>
Qwen2-VL-2B	<i>Retain History 10% / Current 100%</i>			
TAR w/ Uniform	66.2	64.6	65.4	92.6%
<b>TAR (Ours)</b>	<b>66.9</b>	<b>66.0</b>	<b>66.5</b>	<b>94.2%</b>

**Table 4: Comparison of spatial sampling strategies for current frame pruning. We assess SSP with uniform grid sampling versus random sampling.**

Method	AITW	GUI-Ody	Avg.	Rel.
Qwen2-VL-2B	<i>Upper Bound (Full Tokens)</i>			
Vanilla	69.5	71.8	70.6	100%
Qwen2-VL-2B	<i>Retain History 100% / Current 75%</i>			
SSP w/ Random	66.5	69.4	68.0	96.3%
<b>SSP (Ours)</b>	<b>67.7</b>	<b>69.8</b>	<b>68.8</b>	<b>97.4%</b>
Qwen2-VL-2B	<i>Retain History 100% / Current 60%</i>			
SSP w/ Random	64.9	66.1	65.5	92.8%
<b>SSP (Ours)</b>	<b>66.3</b>	<b>66.7</b>	<b>66.5</b>	<b>94.2%</b>
Qwen2-VL-2B	<i>Retain History 100% / Current 45%</i>			
SSP w/ Random	60.8	60.8	60.8	86.1%
<b>SSP (Ours)</b>	<b>61.7</b>	<b>61.4</b>	<b>61.6</b>	<b>87.3%</b>

which modulates the trade-off between local saliency and global

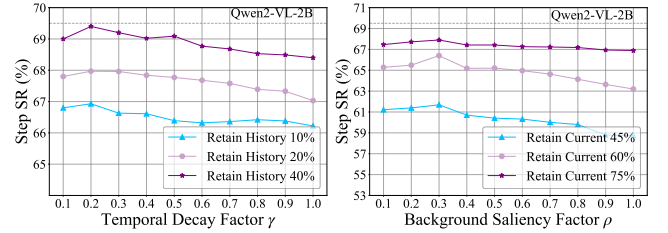


**Figure 5: Hyperparameter sensitivity analysis on AITW. We evaluate the Step SR under varying compression intensities: the impact of the temporal decay factor  $\gamma$  in TAR, and the impact of the background saliency factor  $\rho$  in SSP.**

structure. Figure 5 (Right) reveals a distinct peak at  $\rho = 0.3$ . Deviations cause degradation: higher  $\rho$  sacrifices layout integrity, while lower  $\rho$  captures insufficient semantic context, verifying that a balanced allocation is critical.

**Pruning Layer Depth ( $L$ ).** With retention ratios fixed at  $\lambda = 0.1$  and  $\mu = 0.75$ , we systematically investigate the efficiency-performance trade-off by varying the pruning layer insertion depth  $L$ . As shown in Table 5, results reveal a distinct non-monotonic trend. Pruning at the earliest stage ( $L = 1$ ) precipitates a performance collapse (12.4% Step SR) accompanied by an anomalous surge in FLOPs (3.79T). We attribute this to the immature attention patterns in the first layer, which fail to reliably distinguish interactive semantic regions. This leads to severe grounding hallucinations and output formatting errors, triggering verbose, incorrect generation that paradoxically inflates the total computational cost. In contrast, Layer 2 emerges as the optimal operating point, achieving peak performance (65.3%) while minimizing computational overhead (3.39T). Beyond this point ( $L > 2$ ), performance gradually degrades, and FLOPs linearly increase as additional shallow layers expend resources on the full token sequence before pruning occurs. Qualitative visualizations of attention maps and extended analysis are provided in Appendix D.

## 6 Conclusion

In this paper, we introduce a novel training-free visual token compression framework tailored for high-resolution GUI navigation agents. Specifically, we decouple spatiotemporal redundancy reduction into two synergistic modules: Temporal-Adaptive Resolution (TAR), which dynamically assigns resolution to capture the

**Table 5: Parameter study on the pruning layer depth ( $L$ ) for SSP. We analyze the trade-off between navigation performance (Step SR) and computational cost (FLOPs) by varying the layer index where pruning is executed.**

$L$	1	2	4	8	16
Step SR	12.4	<b>65.3</b>	64.4	61.1	60.6
FLOPs (T)	3.79	<b>3.39</b>	3.45	3.48	3.53

“recency bias” of interactions, and Stratified Structure-aware Pruning (SSP). SSP employs a stratified budget allocation strategy that prioritizes high-attention foreground and background semantics while rigorously safeguarding the global topological layout through uniform grid sampling. Extensive experiments on representative benchmarks demonstrate that our method achieves state-of-the-art performance across Qwen architectures, effectively preventing the catastrophic performance collapse observed in metric-based baselines on sparse, high-resolution screens. Efficiency analysis further confirms that our approach significantly reduces Vision Encoder latency and FLOPs while maintaining superior grounding accuracy, offering a scalable solution that facilitates the practical deployment of real-time MLLMs in resource-constrained edge applications.

## References

- [1] Saeed Ranjbar Alvar, Gursimran Singh, Mohammad Akbari, and Yong Zhang. 2025. Divprune: Diversity-based visual token pruning for large multimodal models. In *Proceedings of the Computer Vision and Pattern Recognition Conference*. 9392–9401.
- [2] Shuai Bai, Keqin Chen, Xuejing Liu, Jialin Wang, Wenbin Ge, Sibao Song, Kai Dang, Peng Wang, Shijie Wang, Jun Tang, et al. 2025. Qwen2. 5-vl technical report. *arXiv preprint arXiv:2502.13923* (2025).
- [3] John Canny. 2009. A computational approach to edge detection. *IEEE Transactions on pattern analysis and machine intelligence* 6 (2009), 679–698.
- [4] Hyungjoo Chae, Namyoun Kim, Kai Tzu-iunn Ong, Minju Gwak, Gwanwoo Song, Jihoon Kim, Sunghwan Kim, Dongha Lee, and Jinyoung Yeo. 2024. Web agents with world models: Learning and leveraging environment dynamics in web navigation. *arXiv preprint arXiv:2410.13232* (2024).
- [5] Ada Chen, Yongjiang Wu, Junyuan Zhang, Jingyu Xiao, Shu Yang, Jen-tse Huang, Kun Wang, Wenxuan Wang, and Shuai Wang. 2025. A Survey on the Safety and Security Threats of Computer-Using Agents: JARVIS or Ultron? *arXiv preprint arXiv:2505.10924* (2025).
- [6] Gongwei Chen, Xurui Zhou, Rui Shao, Yibo Lyu, Kaiwen Zhou, Shuai Wang, Wentao Li, Yinchuan Li, Zhongang Qi, and Liqiang Nie. 2025. Less is more: Empowering gui agent with context-aware simplification. In *Proceedings of the IEEE/CVF International Conference on Computer Vision*. 5901–5911.
- [7] Liang Chen, Haozhe Zhao, Tianyu Liu, Shuai Bai, Junyang Lin, Chang Zhou, and Baobao Chang. 2024. An image is worth 1/2 tokens after layer 2: Plug-and-play inference acceleration for large vision-language models. In *European Conference on Computer Vision*. Springer, 19–35.
- [8] Kanzhi Cheng, Qiushi Sun, Yougang Chu, Fangzhi Xu, Li YanTao, Jianbing Zhang, and Zhiyong Wu. 2024. Seeclick: Harnessing gui grounding for advanced visual gui agents. In *Proceedings of the 62nd Annual Meeting of the Association for Computational Linguistics (Volume 1: Long Papers)*. 9313–9332.
- [9] Filippos Christianos, Georgios Papoudakis, Matthieu Zimmer, Thomas Coste, Zhihao Wu, Jingxuan Chen, Khyati Khandelwal, James Doran, Xidong Feng, Jiacheng Liu, et al. 2023. Pangu-agent: A fine-tunable generalist agent with structured reasoning. *arXiv preprint arXiv:2312.14878* (2023).
- [10] Wenliang Dai, Junnan Li, Dongxu Li, Anthony Tiong, Junqi Zhao, Weisheng Wang, Boyang Li, Pascale N Fung, and Steven Hoi. 2023. Instructblip: Towards general-purpose vision-language models with instruction tuning. *Advances in neural information processing systems* 36 (2023), 49250–49267.
- [11] Truong Hai Dang, Jingyu Xiao, and Yintong Huo. 2025. Envisioning Future Interactive Web Development: Editing Webpage with Natural Language. In *2025 2nd IEEE/ACM International Conference on AI-powered Software (AIware)*. IEEE, 61–66.
- [12] Tri Dao. 2023. Flashattention-2: Faster attention with better parallelism and work partitioning. *arXiv preprint arXiv:2307.08691* (2023).
- [13] Xiang Deng, Yu Gu, Boyuan Zheng, Shijie Chen, Sam Stevens, Boshi Wang, Huan Sun, and Yu Su. 2023. Mind2web: Towards a generalist agent for the web. *Advances in Neural Information Processing Systems* 36 (2023), 28091–28114.
- [14] Zhiqi Ge, Juncheng Li, Xinglei Pang, Minghe Gao, Kaihang Pan, Wang Lin, Hao Fei, Wenqiao Zhang, Siliang Tang, and Yueting Zhuang. 2025. Iris: Breaking gui complexity with adaptive focus and self-refining. In *Proceedings of the IEEE/CVF International Conference on Computer Vision*. 24559–24568.
- [15] Boyu Gou, Ruohan Wang, Boyuan Zheng, Yanan Xie, Cheng Chang, Yiheng Shu, Huan Sun, and Yu Su. 2024. Navigating the digital world as humans do: Universal visual grounding for gui agents. *arXiv preprint arXiv:2410.05243* (2024).
- [16] Kai Han, Yunhe Wang, Hanting Chen, Xinghao Chen, Jianyuan Guo, Zhenhua Liu, Yehui Tang, An Xiao, Chunjing Xu, Yixing Xu, et al. 2022. A survey on vision transformer. *IEEE transactions on pattern analysis and machine intelligence* 45, 1 (2022), 87–110.
- [17] Edward J Hu, Yelong Shen, Phillip Wallis, Zeyuan Allen-Zhu, Yuanzhi Li, Shean Wang, Lu Wang, Weizhu Chen, et al. 2022. Lora: Low-rank adaptation of large language models. *ICLR* 1, 2 (2022), 3.
- [18] Wenbo Hu, Yifan Xu, Yi Li, Weiyue Li, Zeyuan Chen, and Zhuowen Tu. 2024. Bliva: A simple multimodal llm for better handling of text-rich visual questions. In *Proceedings of the AAAI Conference on Artificial Intelligence*, Vol. 38. 2256–2264.
- [19] Alex Kulesza and Ben Taskar. 2012. Determinantal Point Processes for Machine Learning. *Foundations and Trends® in Machine Learning* 5, 2–3 (Dec. 2012), 123–286. doi:10.1561/22000000044
- [20] Hao Li, Qi Lv, Rui Shao, Xiang Deng, Yinchuan Li, Jianye Hao, and Liqiang Nie. 2025. Star: Learning diverse robot skill abstractions through rotation-augmented vector quantization. *arXiv preprint arXiv:2506.03863* (2025).
- [21] Junnan Li, Dongxu Li, Silvio Savarese, and Steven Hoi. 2023. Blip-2: Bootstrapping language-image pre-training with frozen image encoders and large language models. In *International conference on machine learning*. PMLR, 19730–19742.
- [22] Wei Li, William Bishop, Alice Li, Chris Rawles, Folawiyi Campbell-Ajala, Divya Tyamagundlu, and Oriana Riva. 2024. On the effects of data scale on computer control agents. *arXiv e-prints* (2024), arXiv–2406.
- [23] Yanwei Li, Chengyao Wang, and Jiaya Jia. 2024. Llama-vid: An image is worth 2 tokens in large language models. In *European Conference on Computer Vision*. Springer, 323–340.
- [24] Yangfu Li, Hongjian Zhan, Tianyi Chen, Qi Liu, and Yue Lu. 2025. Why 1+1 < 1 in Visual Token Pruning: Beyond Naive Integration via Multi-Objective Balanced Covering. *arXiv preprint arXiv:2505.10118* (2025).
- [25] Zaijing Li, Yuquan Xie, Rui Shao, Gongwei Chen, Dongmei Jiang, and Liqiang Nie. 2024. Optimus-1: Hybrid multimodal memory empowered agents excel in long-horizon tasks. *Advances in neural information processing systems* 37 (2024), 49881–49913.
- [26] Kevin Qinghong Lin, Linjie Li, Difei Gao, Zhengyuan Yang, Shiwei Wu, Zechen Bai, Stan Weixian Lei, Lijuan Wang, and Mike Zheng Shou. 2025. Showui: One vision-language-action model for gui visual agent. In *Proceedings of the Computer Vision and Pattern Recognition Conference*. 19498–19508.
- [27] Junliang Liu, Jingyu Xiao, Wenxin Tang, Wenxuan Wang, Zhixian Wang, Minrui Zhang, and Shuanghe Yu. 2025. Benchmarking MLLM-based Web Understanding: Reasoning, Robustness and Safety. *arXiv preprint arXiv:2509.21782* (2025).
- [28] Tao Liu, Chongyu Wang, Rongjie Li, Yingchen Yu, Xuming He, and Bai Song. 2025. GUI-Rise: Structured Reasoning and History Summarization for GUI Navigation. *arXiv preprint arXiv:2510.27210* (2025).
- [29] Quanfeng Lu, Wenqi Shao, Zitao Liu, Lingxiao Du, Fanqing Meng, Boxuan Li, Botong Chen, Siyuan Huang, Kaipeng Zhang, and Ping Luo. 2025. GUIOdyssey: A comprehensive dataset for cross-app GUI navigation on mobile devices. In *Proceedings of the IEEE/CVF International Conference on Computer Vision*. 22404–22414.
- [30] Dang Nguyen, Jian Chen, Yu Wang, Gang Wu, Namyong Park, Zhengmian Hu, Hanjia Lyu, Junda Wu, Ryan Aponte, Yu Xia, et al. 2025. Gui agents: A survey. In *Findings of the Association for Computational Linguistics: ACL 2025*. 22522–22538.
- [31] Ajay Patel, Markus Hofmarcher, Claudiu Leoveanu-Condrei, Marius-Constantin Dinu, Chris Callison-Burch, and Sepp Hochreiter. 2024. Large language models can self-improve at web agent tasks. *arXiv preprint arXiv:2405.20309* (2024).
- [32] Zehan Qi, Xiao Liu, Iat Long Long, Hanyu Lai, Xueqiao Sun, Wenyi Zhao, Yu Yang, Xinyue Yang, Jiadao Sun, Shuntian Yao, et al. 2024. Webrl: Training llm web agents via self-evolving online curriculum reinforcement learning. *arXiv preprint arXiv:2411.02337* (2024).
- [33] Jeff Rasley, Samyam Rajbhandari, Olatunji Ruwase, and Yuxiong He. 2020. DeepSpeed: System optimizations enable training deep learning models with over 100 billion parameters. In *Proceedings of the 26th ACM SIGKDD international conference on knowledge discovery & data mining*. 3505–3506.
- [34] Christopher Rawles, Alice Li, Daniel Rodriguez, Oriana Riva, and Timothy Lillcrap. 2023. Androidinthewild: A large-scale dataset for android device control. *Advances in Neural Information Processing Systems* 36 (2023), 59708–59728.
- [35] Mauricio GC Resende, Rafael Marti, Micael Gallego, and Abraham Duarte. 2010. GRASP and path relinking for the max–min diversity problem. *Computers &*

*Operations Research* 37, 3 (2010), 498–508.

- [36] Ali M Reza. 2004. Realization of the contrast limited adaptive histogram equalization (CLAHE) for real-time image enhancement. *Journal of VLSI signal processing systems for signal, image and video technology* 38, 1 (2004), 35–44.
- [37] Wenxin Tang, Jingyu Xiao, Wenxuan Jiang, Xi Xiao, Yuhang Wang, Xuxin Tang, Qing Li, Yuehe Ma, Junliang Liu, Shisong Tang, et al. 2025. SlideCoder: Layout-aware RAG-enhanced Hierarchical Slide Generation from Design. *arXiv preprint arXiv:2506.07964* (2025).
- [38] Yuxuan Wan, Yi Dong, Jingyu Xiao, Yintong Huo, Wenxuan Wang, and Michael R Lyu. 2024. Mrweb: An exploration of generating multi-page resource-aware web code from ui designs. *arXiv preprint arXiv:2412.15310* (2024).
- [39] Yuxuan Wan, Tingshuo Liang, Jiakai Xu, Jingyu Xiao, Yintong Huo, and Michael R Lyu. 2025. Automatically Generating Web Applications from Requirements Via Multi-Agent Test-Driven Development. *arXiv preprint arXiv:2509.25297* (2025).
- [40] Junyang Wang, Haiyang Xu, Haitao Jia, Xi Zhang, Ming Yan, Weizhou Shen, Ji Zhang, Fei Huang, and Jitao Sang. 2024. Mobile-agent-v2: Mobile device operation assistant with effective navigation via multi-agent collaboration. *Advances in Neural Information Processing Systems* 37 (2024), 2686–2710.
- [41] Junyang Wang, Haiyang Xu, Jiabo Ye, Ming Yan, Weizhou Shen, Ji Zhang, Fei Huang, and Jitao Sang. 2024. Mobile-agent: Autonomous multi-modal mobile device agent with visual perception. *arXiv preprint arXiv:2401.16158* (2024).
- [42] Peng Wang, Shuai Bai, Siman Tan, Shijie Wang, Zhihao Fan, Jinze Bai, Keqin Chen, Xuejing Liu, Jialin Wang, Wenbin Ge, et al. 2024. Qwen2-vl: Enhancing vision-language model’s perception of the world at any resolution. *arXiv preprint arXiv:2409.12191* (2024).
- [43] Shuai Wang, Weiwen Liu, Jingxuan Chen, Yuqi Zhou, Weinan Gan, Xingshan Zeng, Yuhan Che, Shuai Yu, Xinlong Hao, Kun Shao, et al. 2024. Gui agents with foundation models: A comprehensive survey. *arXiv preprint arXiv:2411.04890* (2024).
- [44] Zihao Wang, Shaofei Cai, Anji Liu, Yonggang Jin, Jinbing Hou, Bowei Zhang, Haowei Lin, Zhaofeng He, Zilong Zheng, Yaodong Yang, et al. 2024. Jarvis-1: Open-world multi-task agents with memory-augmented multimodal language models. *IEEE Transactions on Pattern Analysis and Machine Intelligence* (2024).
- [45] Zora Zhiruo Wang, Jiayuan Mao, Daniel Fried, and Graham Neubig. 2024. Agent workflow memory. *arXiv preprint arXiv:2409.07429* (2024).
- [46] Zhiyong Wu, Zhenyu Wu, Fangzhi Xu, Yian Wang, Qiushi Sun, Chengyou Jia, Kanzhi Cheng, Zichen Ding, Liheng Chen, Paul Pu Liang, et al. 2024. Os-atlas: A foundation action model for generalist gui agents. *arXiv preprint arXiv:2410.23218* (2024).
- [47] Jingyu Xiao, Jiantong Qin, Shuoqi Li, Man Ho Lam, Yuxuan Wan, Jen tse Huang, Yintong Huo, and Michael R. Lyu. 2026. ComUICoder: Component-based Reusable UI Code Generation for Complex Websites via Semantic Segmentation and Element-wise Feedback. arXiv:2602.19276 [cs.SE] <https://arxiv.org/abs/2602.19276>
- [48] Jingyu Xiao, Ming Wang, Man Ho Lam, Yuxuan Wan, Junliang Liu, Yintong Huo, and Michael R Lyu. 2025. Designbench: A comprehensive benchmark for mllm-based front-end code generation. *arXiv preprint arXiv:2506.06251* (2025).
- [49] Jingyu Xiao, Zhongyi Zhang, Yuxuan Wan, Yintong Huo, Yang Liu, and Michael R Lyu. 2025. EfficientUICoder: Efficient MLLM-based UI Code Generation via Input and Output Token Compression. *arXiv preprint arXiv:2509.12159* (2025).
- [50] Yiheng Xu, Zekun Wang, Junli Wang, Dunjie Lu, Tianbao Xie, Amrita Saha, Doyen Sahoo, Tao Yu, and Caiming Xiong. 2024. Aguis: Unified pure vision agents for autonomous gui interaction. *arXiv preprint arXiv:2412.04454* (2024).
- [51] Shunyu Yao, Jeffrey Zhao, Dian Yu, Nan Du, Izhak Shafran, Karthik R Narasimhan, and Yuan Cao. 2022. React: Synergizing reasoning and acting in language models. In *The eleventh international conference on learning representations*.
- [52] Chi Zhang, Zhao Yang, Jiaxuan Liu, Yanda Li, Yucheng Han, Xin Chen, Zebiao Huang, Bin Fu, and Gang Yu. 2025. Appagent: Multimodal agents as smartphone users. In *Proceedings of the 2025 CHI Conference on Human Factors in Computing Systems*. 1–20.
- [53] Qizhe Zhang, Mengzhen Liu, Lichen Li, Ming Lu, Yuan Zhang, Junwen Pan, Qi She, and Shanghang Zhang. 2025. Beyond Attention or Similarity: Maximizing Conditional Diversity for Token Pruning in MLLMs. *arXiv preprint arXiv:2506.10967* (2025).
- [54] Renshan Zhang, Rui Shao, Gongwei Chen, Miao Zhang, Kaiwen Zhou, Weili Guan, and Liqiang Nie. 2025. Falcon: Resolving visual redundancy and fragmentation in high-resolution multimodal large language models via visual registers. In *Proceedings of the IEEE/CVF International Conference on Computer Vision*. 23530–23540.
- [55] Zhuosheng Zhang and Aston Zhang. 2024. You only look at screens: Multimodal chain-of-action agents. In *Findings of the Association for Computational Linguistics: ACL 2024*. 3132–3149.
- [56] Boyuan Zheng, Boyu Gou, Jihyung Kil, Huan Sun, and Yu Su. 2024. Gpt-4v (ision) is a generalist web agent, if grounded. *arXiv preprint arXiv:2401.01614* (2024).
- [57] Nahid Zokaei, Sanjay Manohar, Masud Husain, and Eva Ferredoes. 2014. Causal Evidence for a Privileged Working Memory State in Early Visual Cortex. *Journal of Neuroscience* 34, 1 (2014), 158–162. arXiv:<https://www.jneurosci.org/content/34/1/158.full.pdf>

## Appendices

### A Details of experimental setup

#### A.1 Model Architecture Details

We now detail the architectural specifics of the foundation models employed in our framework: Qwen2-VL and Qwen2.5-VL.

**Qwen2-VL [42].** Qwen2-VL introduces a Naive Dynamic Resolution mechanism, enabling the processing of images with arbitrary aspect ratios by converting them into variable-length sequences of patches without padding. To capture the spatial structure of these dynamic sequences, it employs Multimodal Rotary Positional Embeddings (M-RoPE), which decompose positional information into temporal, vertical, and horizontal components. Visual features are extracted via a ViT-based encoder and compressed by a factor of four using a  $2 \times 2$  pooling layer before injection into the Qwen2 language backbone.

**Qwen2.5-VL [2].** Building upon the Qwen2.5 language model, this iteration extends the dynamic processing paradigm to the temporal dimension, supporting native dynamic frame rates for efficient video comprehension. While retaining the M-RoPE mechanism and the C-Former-free architecture of its predecessor, Qwen2.5-VL integrates optimized SwiGLU activations and RMSNorm to ensure numerical stability for long-context multimodal reasoning. The architecture is specifically tuned for fine-grained visual grounding, enabling precise coordinate extraction and structured data parsing.

#### A.2 Dataset Details and Preprocessing

We evaluate our framework across four diverse benchmarks covering mobile and web environments. Below, we detail the specific configurations, splitting protocols, and action spaces for each dataset.

**Android In The Wild (AITW) [34].** As a large-scale repository for smartphone navigation, AITW contains approximately 30k distinct instructions and 715k execution trajectories. A critical limitation of the original dataset partition is the potential for data leakage, arising from overlapping instructions and highly correlated trajectories across training and test sets. To ensure a rigorous and unbiased evaluation, we strictly adhere to the *instruction-wise split* protocol proposed by SeeClick [8], which isolates unique instructions to prevent overfitting. Our data processing pipeline mirrors the settings established in SeeClick. The agent operates within a defined action space comprising 12 primitives: Click, Type, Select, Scroll Up/Down/Left/Right, Press Back, Press Home, Press Enter, Status Task Complete, and Status Task Impossible.

**GUI-Odyssey [29].** This dataset serves as a comprehensive benchmark for cross-application navigation, featuring 7,735 episodes collected across six distinct mobile devices to test generalization across hardware variations. We align our data preprocessing and evaluation metrics strictly with the original GUI-Odyssey protocols. However, considering the long-horizon nature of this benchmark—characterized by an average of 15 steps per episode [6]—we conduct our evaluation on a randomly sampled subset comprising one-third of the test set to balance computational efficiency with evaluation rigor. The supported action space consists of 9

distinct operations: Click, Scroll, Long Press, Type, Complete, Impossible, Home, Back, and Recent.

**AndroidControl** [22]. Designed to assess task complexity handling, AndroidControl encompasses 14,548 unique tasks distributed across 833 Android applications. It distinguishes itself by providing both high-level (abstract) and low-level (step-by-step) instructions. For this benchmark, we follow the preprocessing and evaluation standards set by OS-Atlas [46]. The action space includes 9 primitives: Click, Scroll, Long Press, Type, Navigate Home, Navigate Back, Open App, Wait, and Terminate.

**Mind2Web** [13]. Mind2Web features over 2,000 tasks across 137 websites, providing raw HTML observations initially tailored for text-based agents. To bridge the modality gap for Vision-Language Models (VLMs), we render these observations into screenshots accompanied by bounding boxes for interactive elements. Since processing full-page screenshots (which can reach resolutions like  $1920 \times 12000$ ) is computationally prohibitive for current VLMs, we adopt the viewport normalization strategy from SeeClick. Specifically, we crop the view around the target element and standardize the resolution to  $1920 \times 1080$ . The action space for Mind2Web is streamlined to 2 core actions: Click and Type.

### A.3 Comparison methods

To strictly evaluate the effectiveness of our proposed framework, we compare it against four state-of-the-art, training-free visual token pruning methods. These baselines span distinct pruning paradigms, ranging from attention-based filtering to advanced metric-based optimization.

**FastV** [7]. As a pioneer in attention-guided compression, FastV identifies the “inefficient attention” phenomenon where deep layers in MLLMs exhibit sparse attention towards visual tokens. Operating on the hypothesis that tokens receiving low attention scores contribute minimally to semantic reasoning, FastV employs a straightforward filtration strategy. Specifically, it discards visual tokens with the lowest aggregated visual-text attention scores after the second transformer layer. This inference-time pruning mechanism accelerates computation but assumes that attention magnitude is the sole indicator of token importance.

**DivPrune** [1]. Distinct from attention-centric approaches, DivPrune addresses visual redundancy through the lens of geometric diversity. It formulates the token selection process as a Max-Min Diversity Problem (MMDP). Rather than relying on semantic alignment, DivPrune aims to maximize the minimum pairwise distance among the retained tokens. By enforcing spatial separation in the feature space, it seeks to preserve a subset of tokens that are maximally distinct from one another, thereby ensuring broad coverage of the visual field and mitigating the risk of representational collapse.

**CDPruner** [53]. This method argues that relying solely on visual similarity or attention scores leads to suboptimal instruction adherence. CDPruner introduces the concept of “Conditional Diversity” to bridge this gap. It reformulates the pruning task using a Determinantal Point Process (DPP), a probabilistic framework used to model repulsion between items. By constructing a kernel that conditions visual similarity on the specific textual instruction, CDPruner selects a subset of tokens that maximizes the determinant of the kernel matrix. This approach statistically guarantees that

the retained tokens offer high coverage of the image content while remaining strictly relevant to the user’s query.

**MoB** [24]. MoB provides a rigorous theoretical grounding for token pruning by modeling it as a bi-objective  $\epsilon$ -covering problem based on the Hausdorff distance. It identifies an intrinsic trade-off between two competing objectives: prompt alignment and visual preservation. To resolve this, MoB derives a closed-form error bound and employs a greedy radius-trading algorithm to optimize the budget allocation dynamically. This method ensures that the selected tokens form a comprehensive cover of the original feature manifold, effectively balancing the reconstruction of visual details with the extraction of instruction-relevant features under strict budget constraints.

### A.4 Implementation Details

**Hardware Setup.** Fine-tuning was performed on a computational node equipped with four NVIDIA A100 GPUs (80GB), leveraging DeepSpeed ZeRO-2 [33] and FlashAttention-2 [12] with `bf16` precision. In contrast, all inference and efficiency evaluations were conducted on a single NVIDIA RTX 4090 (24GB) to assess performance on consumer-grade hardware.

**Base Models.** We employ **Qwen2-VL-2B** and **Qwen2.5-VL-7B** as our foundational backbones. These models were selected for their state-of-the-art visual understanding capabilities and dynamic resolution support.

**Visual Input Configuration.** To balance the trade-off between temporal context and visual resolution under GPU constraints, we follow the visual input configuration set by SimpAgent [6]. For AITW and GUI-Odyssey, we incorporate 4 historical frames. Furthermore, we apply a global low-resolution setting, where the longest edge of all input images is uniformly rescaled to 512 pixels. Conversely, for AndroidControl and Mind2Web, where discerning fine-grained UI elements is critical, we prioritize visual fidelity over sequence length, retaining 2 high-resolution historical frames.

**Fine-tuning Strategy.** To align the general-purpose MLLMs with the specific action formatting requirements of each dataset, we performed Supervised Fine-Tuning (SFT) using Low-Rank Adaptation (LoRA) [17]. We applied LoRA adapters exclusively to the language model components (linear layers in the attention mechanism) with a rank  $r = 8$  and a scaling factor  $\alpha = 16$ . Crucially, since our primary objective during this stage is format adaptation rather than injecting new knowledge, we standardized the training duration to 2 **epochs** across all datasets to prevent overfitting and preserve the pre-trained model’s generalization abilities.

**A.4.1 Hyperparameter Settings.** We tailored the optimization settings (Batch Size and Learning Rate) for each benchmark to accommodate varying image resolutions and dataset complexities. The configurations on our  $4 \times$  A100 cluster were set as follows:

- **AITW:** We employed a learning rate of  $3e-5$ . The per-device batch size was set to 8 with a gradient accumulation step of 1, resulting in a global batch size of 32.
- **Mind2Web:** Given the high resolution of web screenshots, we used a learning rate of  $5e-4$ . We reduced the per-device batch size to 2 with a gradient accumulation step of 1, resulting in a global batch size of 8.

- **GUI-Odyssey:** We utilized a learning rate of  $3e-5$ . The per-device batch size was set to 4 with 4 gradient accumulation steps, yielding a global effective batch size of 64.
- **AndroidControl:** To handle the task complexity, we employed a higher learning rate of  $3e-4$ . We used a per-device batch size of 2 combined with 16 gradient accumulation steps, resulting in a global batch size of 128.

**A.4.2 Prompt Construction.** To enable the model to reason about sequential interactions, we organize the input data as an interleaved sequence of historical screenshots and past actions, culminating in the current observation and the natural language instruction. We adopt a structured prompt format where actions are parsed into a JSON-compatible string containing the `action_type` and specific arguments.

The specific template for instruction fine-tuning is illustrated in **Box 1**.

#### Box 1: Instruction Prompt Template

```
"Please generate the next move according to the
instruction, previous actions, previous ui screenshot
and current ui screenshot.
Instruction: What time is it in Paris?.
Image_0: <image>
Step_0: {"action_type": "Scroll Down"}.
Image_1: <image>
Step_1: {"action_type": "Click", "click_point":
(545,748)}.
Image_2: <image>
Step_2: {"action_type": "Press Home"}.
Image_3: <image>
Step_3: {"action_type": "Click", "click_point":
(608,669)}.
Image_4: <image>"
```

**A.4.3 Edge Detection.** To efficiently categorize visual tokens into foreground ( $\mathcal{T}_{fg}$ ) and background ( $\mathcal{T}_{bg}$ ) sets, we employ a light-weight, training-free detection pipeline tailored for GUI elements. The procedure consists of three stages:

**1. Preprocessing.** The input RGB image is converted to grayscale and smoothed using a Gaussian filter ( $5 \times 5$  kernel) to suppress sensor noise. Crucially, to handle varying contrast levels across different applications, we apply Contrast Limited Adaptive Histogram Equalization (CLAHE) [36] to enhance local boundary definitions before detection.

**2. Multi-scale Edge Extraction.** We utilize the Canny [3] edge detector with dual-threshold hysteresis. To ensure robustness, we compute edges at two sensitivity levels and merge the results via a bitwise OR operation. Subsequently, a morphological closing operation (using a  $3 \times 3$  rectangular kernel) is applied to bridge disconnected edge fragments and ensure structural continuity of UI widgets.

**3. Token Masking.** Valid contours are filtered based on area and aspect ratio constraints to eliminate pixel-level artifacts. The resulting binary occupancy mask is then downsampled to the Vision

---

#### Algorithm 1 Temporal-Adaptive Resolution (TAR)

---

```
1: Input: History context  $\mathcal{H}_t = \{X_{t-1}, \dots, X_{t-T}\}$ , Original token
count  $N_{orig}$ , History retention ratio  $\lambda$ , Decay factor  $\gamma$ .
2: Output: Resized history frames  $\mathcal{H}'_t$ .
3: PHASE 1: Calculate Global Budget
4:  $N_{budget} \leftarrow \lfloor T \times N_{orig} \times \lambda \rfloor$ 
5: Initialize total weight sum  $W_{sum} \leftarrow 0$ 
6: Initialize empty list for weights  $\mathbf{w} \leftarrow []$ 
7: PHASE 2: Compute Linear Decay Weights
8: for  $k = 1$  to  $T$  do
9:    $w_k \leftarrow \gamma + (1 - \gamma) \frac{T-k}{T-1}$  {Higher weight for recent frames
   ( $k \rightarrow 1$ )}
10:  Append  $w_k$  to  $\mathbf{w}$ 
11:   $W_{sum} \leftarrow W_{sum} + w_k$ 
12: end for
13: PHASE 3: Allocate and Resize
14:  $\mathcal{H}'_t \leftarrow \emptyset$ 
15: for  $k = 1$  to  $T$  do
16:    $n_k \leftarrow N_{budget} \cdot \frac{w_k}{W_{sum}}$  {Token quota for frame  $t - k$ }
17:    $s_k \leftarrow \sqrt{\frac{n_k}{N_{orig}}}$  {Derive spatial scaling factor}
18:    $X'_{t-k} \leftarrow \text{Resize}(X_{t-k}, s_k)$  {Bilinear interpolation}
19:   Add  $X'_{t-k}$  to  $\mathcal{H}'_t$ 
20: end for
21: return  $\mathcal{H}'_t$ 
```

---

Transformer’s patch grid via max-pooling, assigning a token to  $\mathcal{T}_{fg}$  if its corresponding patch contains any valid structural edge.

## B Detailed Algorithms

In this section, we provide the pseudocode for the two core components of our GUIPruner framework: the **Temporal-Adaptive Resolution (TAR)** mechanism (Algorithm 1) and the **Stratified Structure-aware Pruning (SSP)** strategy (Algorithm 2). These algorithms detail the procedural implementation of the global-to-local resource scheduling and the topology-preserving token selection described in the main text.

## C SSP Visualization

Figure 6 illustrates the hierarchical token selection process of our SSP module on a **Mind2Web** sample, utilizing the **Qwen2.5-VL-7B** backbone. We configure the current frame retention rate at  $\mu = 0.45$  and the background saliency factor at  $\rho = 0.3$ . The visualization demonstrates the three-stage stratification: (1) **Foreground tokens (Red)** representing interactive primitives (e.g., input fields, buttons) are prioritized; (2) **Background tokens (Green)** are selected based on saliency scores to capture local context; (3) **Uniform Grid tokens (Blue)** fill the remaining budget to preserve the global topological layout.

## D Analysis of Pruning Depth

In the main text, we identified a critical "performance collapse" at pruning depth  $L = 1$  (12.4% Step SR) and an optimal operating point at Layer 2 ( $L = 2$ ). To elucidate the mechanism governing this non-monotonic trend, we visualize the attention heatmaps of

**Algorithm 2** Stratified Structure-aware Pruning (SSP)

---

```

1: Input: Visual token sequence  $\mathcal{T}$ , Global retention ratio  $\mu$ , Back-
   ground saliency factor  $\rho$ .
2: Output: Compressed token sequence  $\mathcal{T}_{final}$ .
3: PHASE 1: Partition and Estimation
4:  $\mathcal{T}_{fg}, \mathcal{T}_{bg} \leftarrow \text{EdgeDetectionPartition}(\mathcal{T})$ 
5: Compute importance scores  $\{s_i\}$  for all  $t_i \in \mathcal{T}$  using shallow
   layer attention.
6: PHASE 2: Determine Budget Constraints
7:  $K_{total} \leftarrow \lfloor |\mathcal{T}| \times \mu \rfloor$ 
8: PHASE 3: Hierarchical Retention
9:  $\triangleright$  Foreground Saliency Preservation
10:  $K_{fg} \leftarrow \lfloor |\mathcal{T}_{fg}| \times \mu \rfloor$ 
11:  $\mathcal{S}_{fg} \leftarrow \text{TopK}(\mathcal{T}_{fg}, K_{fg}, \text{key} = s_i)$ 
12:  $\triangleright$  Background Semantic Retention
13:  $K_{bg} \leftarrow \lfloor |\mathcal{T}_{bg}| \times (\mu \cdot \rho) \rfloor$ 
14:  $\mathcal{S}_{bg} \leftarrow \text{TopK}(\mathcal{T}_{bg}, K_{bg}, \text{key} = s_i)$ 
15:  $\triangleright$  Topological Structure Completion
16:  $K_{res} \leftarrow K_{total} - (|\mathcal{S}_{fg}| + |\mathcal{S}_{bg}|)$ 
17:  $\mathcal{T}_{remain} \leftarrow \mathcal{T} \setminus (\mathcal{S}_{fg} \cup \mathcal{S}_{bg})$ 
18:  $\mathcal{S}_{uni} \leftarrow \text{UniformGridSampling}(\mathcal{T}_{remain}, K_{res})$  {Safeguard
   global layout}
19: PHASE 4: Final Aggregation
20:  $\mathcal{T}_{final} \leftarrow \mathcal{S}_{fg} \cup \mathcal{S}_{bg} \cup \mathcal{S}_{uni}$ 
21: return  $\mathcal{T}_{final}$ 

```

---

the Large Language Model (LLM) across varying encoder depths ( $L \in \{1, 2, 4, 8, 16\}$ ). Figure 7 illustrates these dynamics for two query-driven scenarios where the interaction target is the search bar.

**Layer 1: Spatial Misalignment.** As observed in the first column of Figure 7, the attention distribution at  $L = 1$  exhibits severe spatial misalignment. Although the attention is not globally dispersed, it fails to accurately localize the task-relevant region.

- Instead of focusing on the search bar required by the instruction, the attention hotspots (red/yellow regions) land on irrelevant local features or peripheral edges.

This phenomenon confirms that at Layer 1, the visual tokens have not yet effectively integrated with the textual instruction to guide localization. Consequently, pruning based on this misaligned map indiscriminately discards the critical search bar tokens while retaining irrelevant noise, directly leading to the performance collapse observed in our experiments.

**Layer 2: Precise Target Alignment (The Sweet Spot).** A distinct correction occurs at Layer 2. The attention mechanism successfully fuses the instruction with visual features, correcting the spatial deviation.

- As shown in the second column, the attention focus shifts decisively to cover the search bar, aligning perfectly with the interaction target.

This precise localization allows the SSP module to retain exactly the tokens representing the interactive component while filtering out the rest. This high "signal-to-noise" ratio in token selection explains why  $L = 2$  achieves the peak success rate of 65.3%.

**Table 6: Efficiency comparison on Qwen2.5-VL-7B (AITW dataset, 4 history frames, RTX 4090). We report the number of tokens, FLOPs, Encoder latency, Prefill latency, and GPU memory usage. Bold indicates the best performance.**

Method	# Token	FLOPs (T)	Encoder Time (ms)	Prefill Time (ms)	GPU Memory (MB)
Qwen2.5-VL-7B	1320	27.5	308.7	156.3	18004
FastV	310	13.8 (×2.0)	308.7 (×1.0)	59.1 (×2.6)	17680
DivPrune	310	12.7 (×2.2)	308.7 (×1.0)	53.6 (×2.9)	16616
CDPruner	310	12.7 (×2.2)	308.7 (×1.0)	53.8 (×2.9)	16614
MoB	310	13.8 (×2.0)	308.7 (×1.0)	58.4 (×2.7)	16768
<b>GUIPruner</b>	310	<b>8.9 (×3.1)</b>	<b>97.7 (×3.2)</b>	<b>52.8 (×3.0)</b>	<b>16386</b>

**Layers 4–16: Contextual Diffusion.** Contrary to the assumption that deeper layers yield superior pruning masks, our visualizations (Columns 3–5) reveal a trend of contextual diffusion.

- Starting from Layer 4, the attention focus begins to expand from the precise search bar to encompass the broader global context (e.g., the content results below the bar).

While this expansion reflects the model’s effort to understand the global page semantics, it is detrimental to the specific task of discriminative pruning. By assigning high importance scores to a larger area of the screen, the pruner becomes less selective, retaining redundant background tokens that do not contribute to the immediate interaction. This loss of fine-grained precision, coupled with the increased computational overhead of processing more layers, accounts for the gradual degradation in navigation performance at deeper layers.

## E Efficiency Analysis

To validate the scalability of our framework, we conducted a systematic benchmarking of computational overhead using Qwen2.5-VL-7B on the AITW benchmark with  $N = 4$  history frames. As detailed in Table 6, with retention rates set to  $\lambda = 0.1$  and  $\mu = 0.75$ , our method achieves a 3.1× reduction in FLOPs compared to the original model. Crucially, this theoretical gain translates into tangible speedups: we accelerate the Vision Encoder and Prefill stages by 3.2× and 3.0×, respectively, effectively dismantling the visual encoding bottleneck that constrains prior baselines. Beyond latency, our approach demonstrates exceptional resource efficiency, capping peak GPU memory usage at just 16.4 GB. Consequently, GUIPruner establishes a superior efficiency-performance trade-off compared to competing methods even on larger-scale backbones.

## F Qualitative Analysis

We visualize the retained visual tokens to qualitatively benchmark GUIPruner against state-of-the-art baselines (FastV, DivPrune, CDPruner, and MoB). Experiments are conducted using the Qwen2.5-VL-7B backbone on AITW (Figure 8) and Mind2Web (Figure 9) datasets, with retention rates set to  $\lambda = 0.2$  (history) and  $\mu = 0.45$  (current).

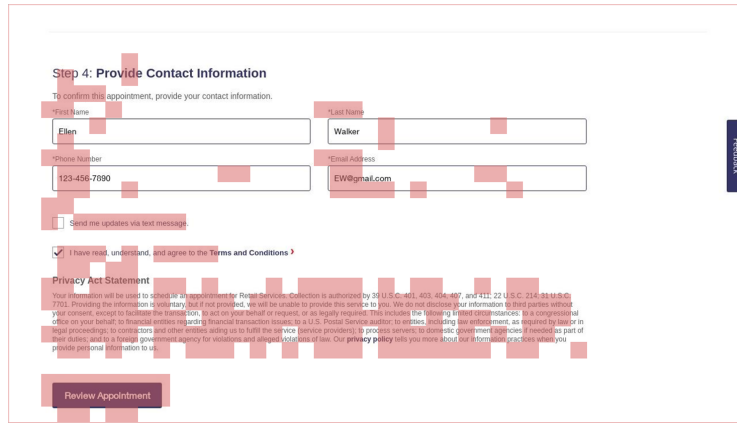
**Structural Integrity in History.** For the history columns (left), baseline methods produce highly fragmented representations. This spatial disruption severs the connection between related UI elements (e.g., a button and its label). In contrast, GUIPruner preserves global structural integrity. By employing a holistic downsampling

strategy rather than sparse token selection, our method maintains the semantic layout. This ensures robust sequential reasoning, even at high compression rates.

**Balanced Coverage in Current Observations.** Current Frame (Right): Unlike baselines that **over-emphasize** salient regions at the cost of global context, our Stratified Structure-aware Pruning (SSP) balances detailed foregrounds with a structured background. It prioritizes actionable tokens via edge priors while maintaining a uniform grid for the remaining areas. This strategy prevents layout fragmentation, ensuring the vision encoder retains the global spatial integrity essential for precise coordinate grounding.

## G Limitations

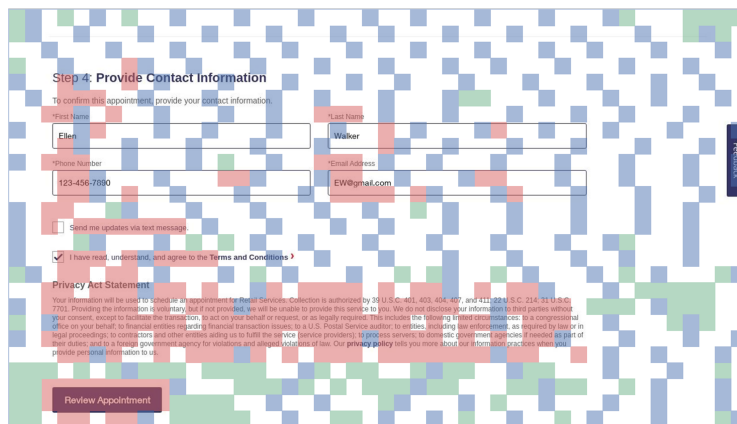
While GUIPruner establishes a new state-of-the-art in efficient visual navigation, it operates within the constraints of the information bottleneck. As indicated by our ablation analysis, there exists a theoretical lower bound to token reduction; applying pruning at extremely shallow layers or enforcing aggressive compression ratios inevitably risks discarding fine-grained visual cues essential for pixel-level grounding. Consequently, performance degradation is unavoidable when pushing compression beyond the Pareto-optimal frontier. Future work implies exploring more adaptive, instance-aware mechanisms to further optimize this trade-off in highly complex visual scenarios.



Foreground Token



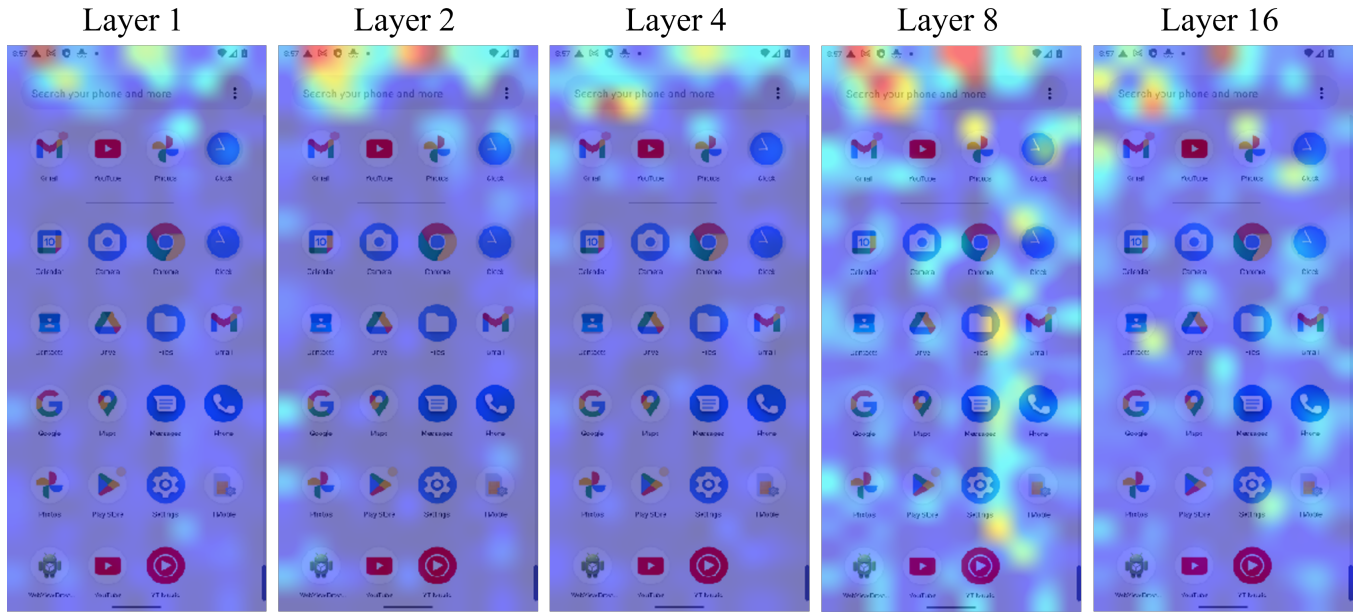
+ Background Token



+ Uniform Sampled Token

Figure 6: Visualizing the SSP Process. A step-by-step breakdown of token retention. The method progressively layers Foreground (Red), Saliency-based Background (Green), and Uniform Grid (Blue) tokens. This guarantees that both fine-grained interactive elements and the coarse-grained global layout are preserved for the VLM.

### Goal: What's the news in Indonesia?



### Goal: What's the weather like in Singapore?

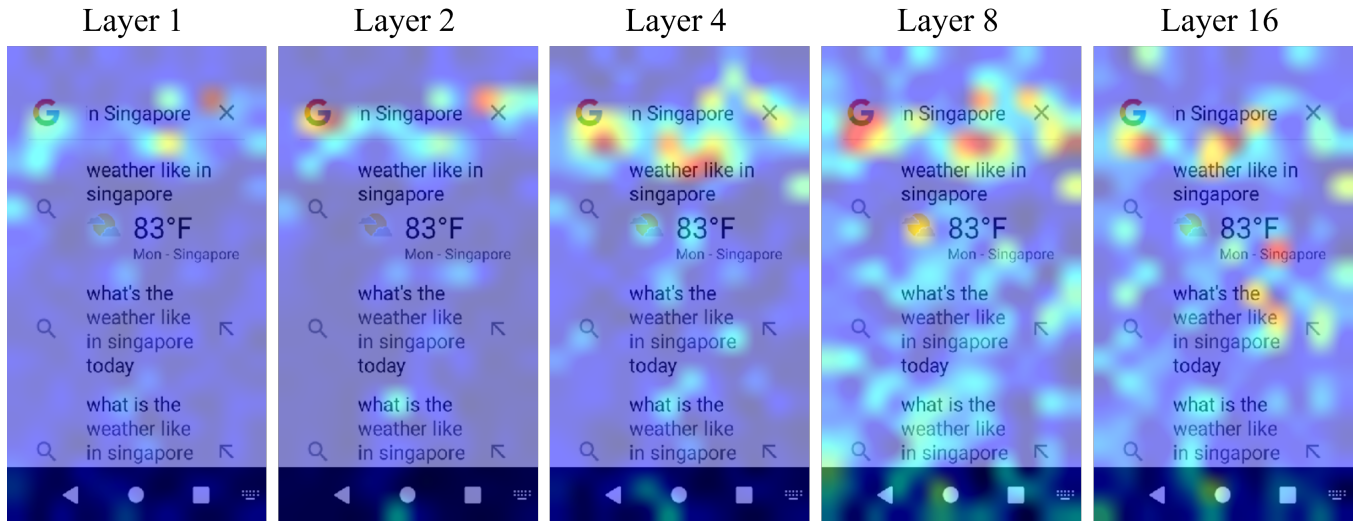


Figure 7: Evolution of LLM Attention Dynamics across Pruning Depths. The heatmaps illustrate the LLM's visual attention for search-related queries. (L1) Attention is misaligned, failing to cover the target search bar. (L2) Attention is precisely focused on the search bar, providing the most accurate signal for token pruning. (L4–L16) Attention progressively expands to the global context, reducing the selectivity required for efficient pruning.



Figure 8: Visualization on AITW (Mobile GUI). Qualitative comparison demonstrating that baselines produce fragmented, spatially disjoint patterns. In contrast, GUIPruner preserves the global layout integrity of history frames and enforces a uniform, structure-aware topology for the current frame.

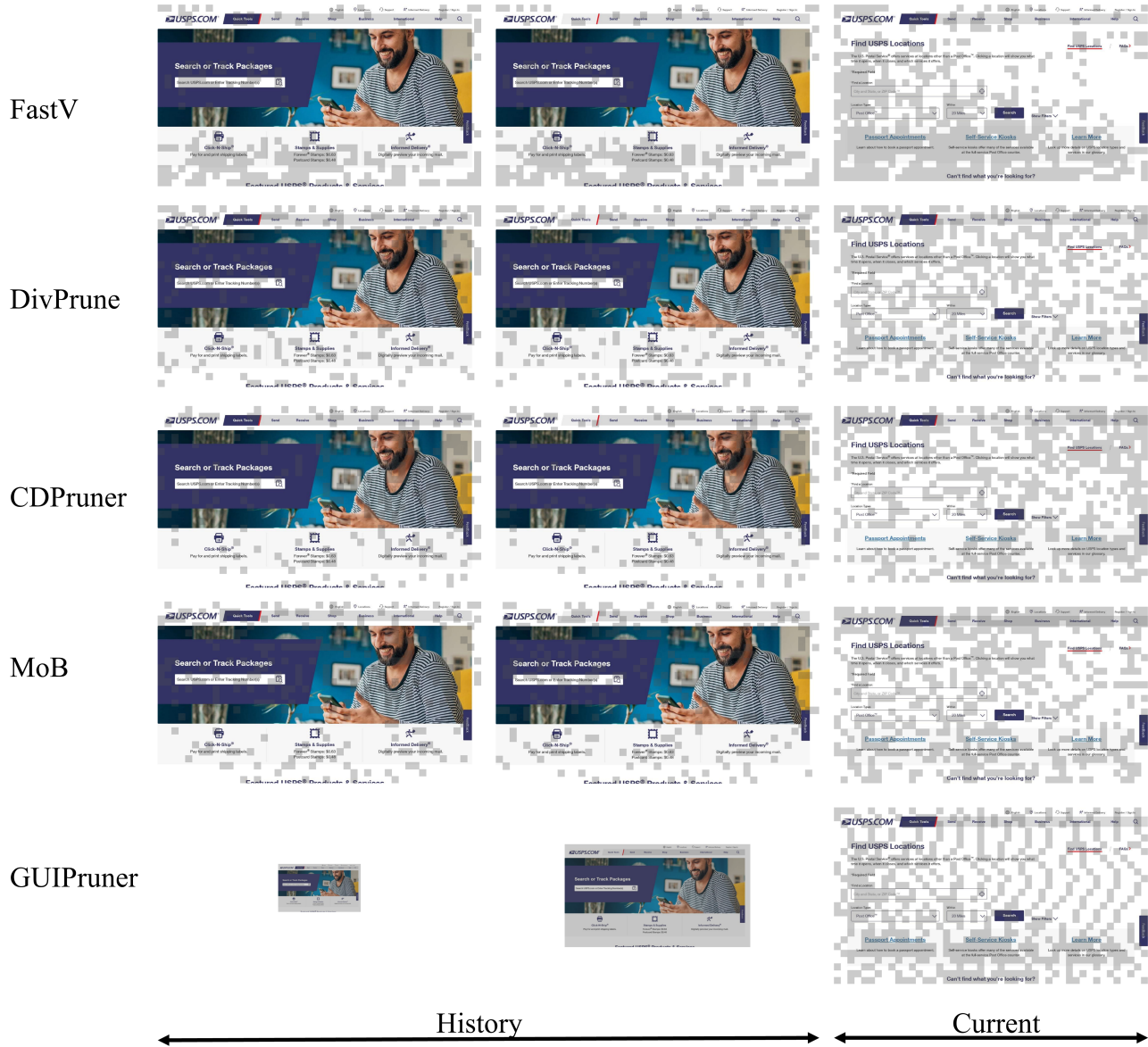


Figure 9: Visualization on Mind2Web (Web GUI). Qualitative comparison demonstrating that GUIPruner effectively preserves the global layout of historical webpages while precisely highlighting interactive elements in the current frame, mitigating the spatial fragmentation observed in baselines.